Contract Report GL-96-1
August 1996

US Army Corps of Engineers
Waterways Experiment Station

In Situ Seismic Investigation of Liquefaction Potential of Soils

by Richard D. Rechtien

Prepared for Headquarters, U.S. Army Corps of Engineers

Contract Report GL-96-1
August 1996

In Situ Seismic Investigation of Liquefaction Potential of Soils

by Richard D. Rechtien

Consulting Geophysicist
15040 County Road 8160
Rolla, MO 65401

Final report

Approved for public release; distribution is unlimited

Prepared for U.S. Army Corps of Engineers
Washington, DC 20314-1000

Under Contract DACW39-95-M-2999

Monitored by U.S. Army Engineer Waterways Experiment Station
3909 Halls Ferry Road, Vicksburg, MS 39180-6199

US Army Corps of Engineers
Waterways Experiment Station

FOR INFORMATION CONTACT :
PUBLIC AFFAIRS OFFICE
U. S. ARMY ENGINEER
WATERWAYS EXPERIMENT STATION
3909 HALLS FERRY ROAD
VICKSBURG, MISSISSIPPI 39180-6199
PHONE : (601)634-2502

Waterways Experiment Station Cataloging-in-Publication Data

Rechtien, Richard D.

In situ seismic investigation of liquefaction potential of soils / by Richard Rechtien ; prepared for U.S. Army Corps of Engineers ; monitored by U.S. Army Engineer Waterways Experiment Station.

46 p. : ill. ; 28 cm. -- (Contract report ; GL-96-1)

Includes bibliographical references.

1. Soil liquefaction -- Measurement. 2. Shear strength of soils -- Measurement. 3. Seismic refraction method. 4. Shear waves -- Measurement. I. United States. Army. Corps of Engineers. II. U.S. Army Engineer Waterways Experiment Station. III. Geotechnical Laboratory (U.S. Army Engineer Waterways Experiment Station) IV. Title. V. Series: Contract report (U.S. Army Engineer Waterways Experiment Station) ; GL-96-1.

TA7 W34c no.GL-96-1

CONTENTS

Preface iv
Conversion Factors, Non-SI to SI Units of Measurement v
1 Introduction 1

Background and Scope 1

2 Relevant Soil Parameters 3

3 Seismic Earth Models 5

Overview 5
Models for Forward Wavefield Calculations 5

4 Inversion of Seismic Data 9

Limited Scope of Inversion Methods 9
Waveform Tomography 10
Diffraction Tomography 15
Traveltime/Attenuation Tomography 17
Hybrid Tomography 20
Non-Tomographic Seismic Methods 21

5 Conceptual Field Tests 22

Potential Seismic Methods for Liquefaction Studies 22
Experimental Geometry - CCBS 23
Experimental Geometry - FRW & FLW 27
Conventional Seismic Tests 28

6 Summary 29

7 Conclusions 31

References 33

PREFACE

The work described in this report was performed during the period May to December 1995 by Dr. Richard D. Rechtien, Consulting Geophysicist and Professor Emeritus, University of Missouri at Rolla. The work was performed under Contract No. DACW39-95-M-2999 and funded by the Earthquake Engineering (EQEN) Research Program project, "Geophysical Methods for Site Characterization and Measurement of Seismic Properties," Work Unit No. 33014.

This report was prepared by Dr. Rechtien. Principal Investigators for the EQEN Research Project and technical monitors for this work were Dr. Dwain K. Butler and Mr. Robert F. Ballard, Jr., Earthquake Engineering and Geosciences Division (EEGD), Geotechnical Laboratory (GL), U.S. Army Engineer Waterways Experiment Station (WES). This work was performed under the general supervision of Dr. Arley G. Franklin, Chief, EEGD, and Dr. William F. Marcuson, Director, GL. Dr. Mary Ellen Hynes was EQEN Project Manager.

At the time of publication of this report, Director of WES was Dr. Robert W. Whalin. Commander was COL Bruce K. Howard, EN.

Conversion Factors, Non-SI to SI Units of Measurement

Non-SI units of measurement used in this report can be converted to SI units as follows:

Mutiply	By	To Obtain
feet	0.3048	meters
feet per second	0.3048	meters per second

1 Introduction

Background and Scope of Work

Liquefaction is a term used to describe a process involving the complete loss of shear strength of loose- to medium-dense sand deposits (or other non-cohesive soils) below the water table during the passage of large-amplitude earthquake waves. The existence of such processes in nature is well evidenced by surface observations at many earthquake sites throughout the world (see, for example, Kawasumi 1968, Seed et al. 1990, and CAEE 1995). A primary objective of liquefaction research is the development of indicators, derived from in situ geotechnical measurements, that provide accurate assessment of liquefaction potential of a cohensionless deposit in a given earthquake environment.

Seismic waves of sufficient magnitude to cause liquefaction cannot (generally speaking) be practically produced for in situ liquefaction studies. Consequently, investigations toward identification of relevant source/soil characteristics have essentially been confined to laboratory experimentation on both field and synthetic soil samples. While these studies have provided a good understanding of the mechanisms of the stress/soil dynamic that produces liquefaction, they have not yielded diagnostic liquefaction parameters that are easily measured in situ.

Currently, in situ estimation of liquefaction potential is accomplished using procedures based on the standard penetration test, cone tip penetration resistance, and normalized shear wave velocity (Finn 1995a,b). Such procedures involve three steps (after Finn):

1) Characterizing the dynamic effects of the earthquake.
2) Characterizing the in situ state of the soil.
3) Application of a criterion for the incidence of soil liquefaction.

Step (1) involves equivalencing of anticipated maximum earthquake ground motion and cyclic laboratory excitation test levels and durations. Step (3) involves empirical correlation of in situ test probe results with site specific soil materials that are considered, by supplemental criteria, to be of high liquefaction potential. Step (2) involves development of definitive field techniques that characterize the in situ state of the soil from the

reference viewpoint of laboratory-generated, engineering criterion of soil liquefaction.

This report considers only seismic methods of imaging subsurface soil structure. Primarily focus will be upon Step(2), and secondarily upon Step (3). The specific report objectives encompass the following topics:

1) Evaluation of current seismic methods.
2) Postulation of potential seismic techniques.
3) Conceptual definition of in situ field tests.

The treatment of this subject begins by considering soil parameters that are relevant to the liquefaction problem. Next, since the process of subsurface imaging requires mathematical models of soil structure, current models for lithified and unlithified, saturated and unsaturated media are discussed. A comprehensive treatment of seismic tomography follows, including discussions of potential capabilities and limitations. Finally, with reference to current and near-future data analysis capability, conceptual field tests are presented .

2 Relevant Soil Parameters

In the fluidization process, earthquake wave motion imparts pseudo-cyclic loading to the soil, resulting in compaction. Since water in the pores of the sediment cannot escape quickly enough to accommodate compaction, an increase of porewater pressure results, leading to a reduction of intergrandular stresses between soil particles. For a given intensity of earthquake shaking, liquefaction potential is controlled by the tendency for compaction and capacity for drainage (Finn 1995b).

Cyclic shearing strain is recognized as the prime agent for generating volume changes (i.e., compaction) in saturated cohesionless soils. Shear strain depends on the in situ shear modulus, which, for saturated cohesionless soils, is strongly dependent upon porosity. Drainage, on the otherhand, is a function of in situ permeability, which is also dependent upon porosity. Therefore, porosity, shear modulus and permeability are important soil parameters for the evaluation of in situ liquefaction potential (Finn 1995b).

The shear modulus, however, cannot generally be measured directly. This quantity is given by the product of density and the square of the shear velocity. Shear velocity can be readily measured in situ. If in situ density was also determinable, then the in situ shear modulus could be calculated. Density is also dependent upon porosity and is a parameter used in the calculation of 'relative density'. Relative density is a liquefaction indicator applied to the evaluation of the shearing resistance of sands. Thus, density and relative density are also liquefaction-relevant soil parameters.

A high degree of fluid saturation is required for liquefaction. For a partially saturated soil, compaction can occur without significant pore water pressure development. Consequently, the in situ degree of saturation is an important quantity to be evaluated.

Finally, soil fabric and structure of a deposit provide clues to density, shearing stiffness, shearing resistance, and porosity.

In summary, the following soil parameters are relevant to estimation of liquefaction potential:

1) density
2) relative density
3) shear modulus

4) porosity
5) permeability
6) saturation
7) soil fabric and structure

3 Seismic Earth Models

Overview

Geophysics in general, and seismology in particular, is an interpretive science. In seismology, earth parameters are not measured directly, but are indirectly inferred through comparison of recorded waveform attributes with those derived synthetically through numerical modeling. Consequently, in the application of any seismic method to subsurface exploration, one must of necessity, at the onset, have a specific earth model in mind, compatible with a chosen process for numerical synthesis of seismic data. Due to the complexity of numerical modeling, this earth model will necessarily be simplistic; inherently capable, at best, of reproducing gross, dominant attributes of measured seismic waveforms. Realization of correspondence between field measurements and numerical model data will ultimately depend upon:

1) The degree of inclusion of stress-strain subtleties.
2) Significance of these subtleties relative to modification of the seismic waveform.
3) Validity of assumptions of isotorpy, homogeneity and model dimensionality.
4) Accuracy of numerical simulation of spatial and temporal source characteristics.

Models For Forward Wavefield Calculations

Poroelastic Models

Biot (1962a) presents a unified treatment of the mechanics of deformation and acoustic propagation in porous media. He treats the fluid-solid medium as a complex physical-chemical system with resultant relaxation and viscoelastic properties of a very general nature. For an isotropic, elastic, porous medium, the principal result of this treatment is the field equations describing coupled energy propagation within the porous solid structure and within the fluid. These equations are given by Biot as,

$$2\sum_j \frac{\partial}{\partial x_j}\left[\mu e_{ij}\right] + \frac{\partial}{\partial x_i}\left[\lambda_c e - \alpha M\zeta\right] = \frac{\partial^2}{\partial t^2}\left[\rho u_i + \rho_f w_i\right], \tag{1}$$

and

$$\frac{\partial}{\partial x_i}\left[\alpha M e - M\zeta\right] = \frac{\partial^2}{\partial t^2}\left[\rho_f u_i + m w_i\right] + \frac{\eta}{k}\frac{\partial}{\partial t} w_i, \tag{2}$$

where,

$$e_{ij} = \frac{\partial}{\partial x_j} u_i \;\; ; \;\; e = \sum_i \frac{\partial}{\partial x_i} u_i \;\; ; \zeta = -\sum_i \frac{\partial}{\partial x_i} w_i \;\; ; \;\; w_i = \sigma\left(U_i - u_i\right) \;\; ; \;\; \mu = \mu_r\left(1 + i\delta\right)$$

u_i is the displacement within the skeletal solid,
U_i is the average fluid displacement,
w_i is the flow of the fluid relative to the frame,
μ_r is the dynamic shear modulus,
ρ_f is the density of the fluid,
λ_c is theadiabatic Lame coefficient,
σ is the porosity,
μ is the complex shear modulus,
δ is the specific loss of the skeletal frame for shear,
η is the kinematic viscosity of the fluid,
m is the virtual mass of the skeletal frame,
ρ is the total mass density,
k is the hydraulic coefficient of permeability,
α, M are Biot elastic coefficients (Biot(1941)).

Equation (1) is the result of the application of the principle of conservation of momentum, while (2) can be interpreted as expressing the dynamics of relative motion of the fluid in a frame of reference moving with the solid. These equations were based on a semiphenomenological formulation of the equations of elasticity for a porous aggregate by Biot (1941; 1956a,b,c; 1962a,b), Frenkel (1944), and Gassmann (1951). The hypothesized form of the microscopic constitutive relationships, which resulted in the equations of motion, was confirmed by Burridge and Keller (1981) in their studies of the dynamic equations which govern the behavior of the medium on the microscopic scale. Moreover, through experimental observations, Plona (1980) confirmed a fundamental prediction of Biot's model by his observation of a second compressional wave (referred to as the 'slow wave'). Stoll and Bryan (1970) and Stoll (1974) extended Biot's theory to include dissipation due to the frame by incorporating complex moduli.

Successful applications of Biot's theory to various fields, notably to seismic exploration (e.g., Geertsma 1957; Geertsma and Smit 1961; Gardner, Gardner, and Gregory 1974; Domenico 1974; Rosenbaum 1974;),

marine acoustics (Stoll 1974, 1977, 1980, 1985; Yamamoto 1983; Badiey and Yamamoto 1985; Turgut and Yamamoto 1988; Yamamoto and Turgut 1988; Yamamoto et al. 1989), and attenuation and dispersion of compressional waves (Dutta and Ode 1979,1983; Stoll and Kan 1981; Ogushwitz 1985; Geli , Bard, and Schmitt 1987; Winkler et al. 1987; Rasolofosaon, 1987; Schmitt, Bouchon, and Bonnet 1988; Yamamoto, Nye, and Kuru 1994, 1995) have demonstrated the utility of the model for a variety of poroelastic problems. The model incorporates eight material parameters (considering η/k as a single variable), including the liquefaction-sensitive parameters: density, shear modulus, porosity, and permeability. Soil fabric and structure can be included by specification of spatial variation of material coefficients. Thus, the Biot model is a general formulation of small amplitude (linear stress-strain relation) wave propagation in saturated sediment deposits characterized by an elastic, porous frame. In the forward modeling arena (as opposed to interpretational problems of waveform inversion) the system of equations lends itself readily to waveform calculations by means of finite difference (Hassanzadeh 1991; Zhu and McMechan 1991; Dai, Vafidis, and Kanasewich 1995) and finite-element methods (Zienkiewicz and Shiomo 1984).

Biot-squirt models

In Biot's model, pore fluid is forced to participate in a solid's oscillatory motion by viscous friction and inertial coupling. A different mechanism of fluid flow during seismic and acoustic wave propagation is associated with the squirting of pore fluid out of thin soft cracks as they are deformed by passing seismic waves. Mavko and Nur (1979) have shown that the squirt-flow mechanism results in much higher and realistic attenuation values in partially saturated rocks than those predicted by Biot's mechanism. Mavko and Nur (1975) have suggested that squirt flow may occur even in fully saturated rocks due to fluid flowing between saturated cracks of different orientation. This mechanism has been shown to be responsible for the measured seismic energy losses and velocity dispersion in sedimentary material for both P- and S-waves (e.g., Murphy, Winkler, and Kleinberg 1986; Wang and Nur 1990). Dvorkin and Nur (1993) and Dvorkin, Mavko, and Nur (1995) proposed a combined Biot-squirt (BISQ) model where the Biot elastic frame is replaced with a viscoelastic one. They considered a macroscopically homogeneous rock with pore space that has thin compliant (soft) and stiff portions. At high confining pressure the thin compliant pores close and the observed velocity dispersion is small and can be adequately described by Biot's theory (Mavko and Jizba 1991). However, at small confining pressure the high observed velocity/frequency dispersion and attenuation can be adequately described by the BISQ model.

Modeling Summary

A BISQ model appears to be appropriate for the description of dynamic response of fully or partially saturated porous media to low amplitude seismic wave energy. This model is reducible, by certain assumptions relative to the independent material parameters listed above, to simpler and standard equations of motion encountered in physics. As for example, assuming the medium to be elastic and non-porous, (2) above vanishes, and (1) assumes the form,

$$2\sum_j \frac{\partial}{\partial x_j}\left[\mu e_{ij}\right] + \frac{\partial}{\partial x_i}\left[\lambda_c e\right] = \frac{\partial^2}{\partial t^2}\left[\rho u_i\right]. \qquad (3)$$

This equation can be recognized as the isotropic, heterogeneous wave equation for a perfectly elastic solid. Other equations of motion can be similarly produced by appropriate choices of material parameter behavior.

I conclude, by virtue of the wide application of Biot's theory in the literature and the essential absence of any other widely accepted model, that the BISQ model can be considered the starting point for most scientific inquiries of wave motion in porous, partially or fully saturated, earth materials. The equations of motion, (1) and (2), even modified by inclusion of squirt flow, are amenable to numerical solution by Finite difference methods (e.g., Dai, Vafidis, and Kanasewich 1995). Consequently, forward modeling of stress waves in porous media is a matter of application of known and proven numerical methods, and is not a subject requiring extensive research and development.

4 Inversion of Seismic Data

Limited Scope Of Inversion Methods

In the discussion of seismic inversion techniques, topics of consideration are restrained to the imaging of very near-surface materials typically associated with earthen dam sites. Complex soil structures, with significant variation of material parameters both laterally and vertically, are assumed. Concepts of uniform layered media are not applicable. Consequently, imaging and migration techniques based upon layered model concepts are not considered.

Seismic inversion methods included in the study of liquefaction potential involved direct comparison of measured waveform attributes with corresponding waveforms derived synthetically from a numerical model. These attributes may simply be traveltime of the first arrival, or first arrival amplitude, or phase; they could also be the entire pulse waveforms, or waveform trains. Regardless of character, conformance between measured and synthetic data attributes generally results from iterative manipulation of earth model parameters. This manipulation is exercised in a regular and controlled way by the minimization of some objective data function; the form of which varies in accordance with the particular waveform attribute in question. This manipulation process is called tomography.

Tomographic algorithms generally fall into three classes: waveform, diffraction, or traveltime/attenuation tomography. For waveform tomography, synthetic waveform calculations, based on some current material parameter distribution, must be made by finite difference methods, or some other appropriate modeling procedure. Waveform tomography is then the interactive minimization of an objective function defined in terms of the sum of time integrals of differences between observed waveforms and synthetic waveforms calculated by a forward modeling procedure.

For diffraction tomography, synthetic seismograms are generated by finite difference methods, or some other appropriate modeling procedure, for a background medium void of anomalous parameter distributions. The objective function is then the difference between the uniform background velocity and the anomalous velocity distribution that is calculated by inversion of the scattered field data.

In traveltime (or attenuation) tomography the forward modeling problem is relatively simple and direct, involving traveltime (or attenuation) calculations through a grid of cells, within which wave speed (or attenuation) is specified, by means of ray or wavefront theory. Traveltime (or attenuation) tomography is then the iterative minimization of an objective function, defined in terms of the sum of differences between observed traveltimes (or amplitudes) and traveltimes (or amplitudes) calculate by means of a forward model, for current estimates of the material parameters.

For a comprehensive presentation of tomographic methods the reader is referred to Nolet (1987a), Wu and Toksök (1987), and Tien and Inderwiesen (1994).

Waveform Tomography

Concept Formulation

I begin an overview of tomography by considering first the most general, and perhaps the most potentially powerful, tomographic process. Waveform tomography attempts the extraction of earth parameters from seismic data by the process of fitting synthetic wavetrain elements to observed wavetrain elements within a measured seismic trace, or collection of traces (a seismogram), or a collection of seismograms. Such a process, in principal, encompasses the possibility of determining all material parameters of the model chosen as the best representation of the real earth. Thus, in principal, the possibility exists to simultaneously determine compressional and shear wave velocities and density as a function of position for the elastic wave model (Equation (3)), or all eight independent, spatially variable, material constants for the Biot model (Equations (1) and (2)). I stress the qualifier 'in principal' in that the quality of data, relative significance of parameter influence on the shape of the wavetrain, and the inaccuracy of inversion procedures limit current inversion applications.

Waveform fitting can be described as an inverse problem based upon methods of nonlinear optimization. In general the optimization problem is one of minimizing some nonlinear objective function of the model parameters, which is generally taken to be the difference between observed and predicted seismograms. Inversion is then reduced to the question of how to minimize the objective function. The following is a heuristic presentation of waveform tomography.

A seismogram is acquired as output of discrete sensors distributed somewhere in space. This data is the result of the response of these sensors to incident energy generated at some other discrete point in the same space. This space could be one-, two-, or three-dimensional.

Let $\mathbf{p}$ be an M-dimensional vector of all model parameters (velocity, density, porosity, permeability, etc.); $\psi_i(\mathbf{p},t)$, the i-th synthetic time series calculated by means of model $\mathbf{p}$; N, the total number of seismic time series available; T_i, a (sufficiently large) time span; $s_i(t)$, the i-th observed

seismic time series; and q, the norm. Following Nolet (1987b), the objective function to be minimized is defined by

$$F(\mathbf{p}) = \frac{1}{q}\sum_{i=1}^{N}\int_{0}^{T_i}\left|\mathbf{R}\psi_i(\mathbf{p},t)-\mathbf{R}s_i(t)\right|^{q} dt, \tag{4}$$

where **R** is a desired filtering and/or windowing operator. In the case of traveltime tomography the operator **R** would be unity and the time integral would vanish. Other definitions of the objective function may be used. The reader is referred to Tarantola (1987a).

The inversion process requires certain derivatives with respect to model parameters p_i. First, we form a vector whose elements are given by the derivative $\partial F(\mathbf{p})/\partial p_i$,

$$\mathbf{g}(\mathbf{p}) \equiv \nabla F(\mathbf{p}) = \sum_{i=1}^{N}\int_{0}^{T_i}\mathbf{R}\nabla\psi_i\left[\mathbf{R}\psi_i(\mathbf{p},t)-\mathbf{R}s_i(t)\right]^{q-1} dt. \tag{5}$$

Next we form the Hessian matrix, $\mathbf{H}(\mathbf{p})$, the matrix of second derivatives $\partial^2 F(\mathbf{p})/\partial p_i \partial p_j$,

$$\mathbf{H}(\mathbf{p}) \equiv \nabla\mathbf{g}(\mathbf{p}) = \sum_{i=1}^{N}\int_{0}^{T_i}\Big\{(q-1)\mathbf{R}\nabla\psi_i\left[\mathbf{R}\psi_i(\mathbf{p},t)-\mathbf{R}s_i(t)\right]^{q-2}\left(\mathbf{R}\nabla\psi_i\right)^{\mathrm{T}} \tag{6}$$
$$+\mathbf{R}\nabla\nabla\psi_i\left[\mathbf{R}\psi_i(\mathbf{p},t)-\mathbf{R}s_i(t)\right]^{q-1}\Big\}dt.$$

Nonlinear optimization algorithms work in an iterative way. A starting model **p** is updated with a correction factor $\Delta\mathbf{p}$ to give a new model $\mathbf{p}+\Delta\mathbf{p}$. This new model in then taken as a starting model in the next iteration. Suppose that at some stage we have arrived at the model **p**. With a simple Taylor expansion we may now find an approximation for the step $\Delta\mathbf{p}$ that should bring us close to the minimum of $F(\mathbf{p})$, where $\mathbf{g}(\mathbf{p}) = 0$:

$$F(\mathbf{p}+\Delta\mathbf{p}) \approx F(\mathbf{p}) + \mathbf{g}(\mathbf{p})^{\mathrm{T}}\Delta\mathbf{p} + \frac{1}{2}\Delta\mathbf{p}^{\mathrm{T}}\mathbf{H}(\mathbf{p})\Delta\mathbf{p}. \tag{7}$$

Differentiating (7) with respect to $\Delta\mathbf{p}$ gives:

$$\mathbf{g}(\mathbf{p}+\Delta\mathbf{p}) \approx \mathbf{g}(\mathbf{p}) + \mathbf{H}(\mathbf{p})\Delta\mathbf{p}. \tag{8}$$

So that $\Delta\mathbf{p}$ can be found by setting $\mathbf{g}(\mathbf{p}+\Delta\mathbf{p}) = 0$ and solving:

$$\mathbf{H}(\mathbf{p})\Delta\mathbf{p} = -\mathbf{g}(\mathbf{p}). \tag{9}$$

This is the essence of waveform tomography, however, it is noted that the above presentation is given heuristically (with much liberality relative to mathematical rigor). This was done for the purpose of clarity of process.

For a more rigorous treatment the reader is once again referred to Nolet (1987b) and Tarantola (1987).

For the purpose of illustrating how the vector $\mathbf{g}(\mathbf{p})$ and the Hessian matrix $\mathbf{H}(\mathbf{p})$ are calculated, consider the heterogeneous equations of motion for a solid (non-porous) media, as given by (3):

$$2\sum_j \frac{\partial}{\partial x_j}\left[\mu e_{ij}\right] + \frac{\partial}{\partial x_i}\left[\lambda_c e\right] - \frac{\partial^2}{\partial t^2}\left[\rho u_i\right] = 0. \qquad (3)$$

In this equation there are three material parameters: μ, λ_c, and ρ, which, in general, are a function of the spatial coordinates. Consider further that we approach a solution to this equation, and the partial differential equations to follow, by means of finite differences (see Kelly (1976)).

The elements of $\mathbf{g}(\mathbf{p}) \equiv \nabla F(\mathbf{p})$ are found by applying the operators $\partial/\partial\mu$, $\partial/\partial\lambda_c$, and $\partial/\partial\rho$ successively to Equation (3), resulting in:

$$2\sum_j \frac{\partial}{\partial x_j}\left[\mu \frac{\partial e_{ij}}{\partial \mu}\right] + \frac{\partial}{\partial x_i}\left[\lambda_c \frac{\partial e}{\partial \mu}\right] - \frac{\partial^2}{\partial t^2}\left[\rho \frac{\partial u_i}{\partial \mu}\right] =$$

$$-2\sum_j \frac{\partial}{\partial x_j}\left[e_{ij}\right], \qquad (10a)$$

$$2\sum_j \frac{\partial}{\partial x_j}\left[\mu \frac{\partial e_{ij}}{\partial \lambda_c}\right] + \frac{\partial}{\partial x_i}\left[\lambda_c \frac{\partial e}{\partial \lambda_c}\right] - \frac{\partial^2}{\partial t^2}\left[\rho \frac{\partial u_i}{\partial \lambda_c}\right] = -\frac{\partial e}{\partial x_i}, \qquad (10b)$$

and

$$2\sum_j \frac{\partial}{\partial x_j}\left[\mu \frac{\partial e_{ij}}{\partial \rho}\right] + \frac{\partial}{\partial x_i}\left[\lambda_c \frac{\partial e}{\partial \rho}\right] - \frac{\partial^2}{\partial t^2}\left[\rho \frac{\partial u_i}{\partial \rho}\right] = -\frac{\partial^2 u_i}{\partial t^2}. \qquad (10c)$$

The terms in the R.H.S. of (10) are virtual sources generating, respectively, 'virtual displacements':

$$\frac{\partial \psi_i}{\partial \mu} = \frac{\partial u_i}{\partial \mu};\ \frac{\partial \psi_i}{\partial \lambda_c} = \frac{\partial u_i}{\partial \lambda_c};\ \frac{\partial \psi_i}{\partial \rho} = \frac{\partial u_i}{\partial \rho}, \qquad (11)$$

(since $\partial e_{ij}/\partial\mu = \partial^2 \psi_i / \partial\mu\partial x_j$, etc.), which are the components of the vector $\nabla\psi$ in (5) and (6). By first solving (3) for $u_i(\mathbf{x},t)$, for a given time step within the finite difference iterative time loop, the virtual source terms of (10) can be readily formed. The solutions for the dependent variables

(virtual displacements) (11) can then be obtained and the components of $\mathbf{g}(\mathbf{p})$ formed for the same time step.

To calculate the elements of the Hessian matrix, $\mathbf{H}(\mathbf{p})$, we take derivatives of (10) with respect to all three parameters: μ, λ_c, and ρ. For example, one derivative produces equations of motion for the 'virtual displacement' $\partial^2\psi_i / \partial p \partial u = \partial^2 u_i / \partial \rho \partial \mu$:

$$2\sum_j \frac{\partial}{\partial x_j}\left[\mu \frac{\partial^2 e_{ij}}{\partial \rho \partial \mu}\right] + \frac{\partial}{\partial x_i}\left[\lambda_c \frac{\partial^2 e}{\partial \rho \partial \mu}\right] - \frac{\partial^2}{\partial t^2}\left[\rho \frac{\partial^2 u_i}{\partial \rho \partial \mu}\right] =$$

$$-2\sum_j \frac{\partial}{\partial x_j}\left[\frac{\partial e_{ij}}{\partial \rho}\right] + \frac{\partial^2}{\partial t^2}\left[\frac{\partial u_i}{\partial \mu}\right] \qquad (12)$$

The terms on the R.H.S. of (12) are virtual sources generating virtual displacements: $\partial^2\psi_i / \partial p \partial u = \partial^2 u_i / \partial \rho \partial \mu$. The virtual source terms of (12) can be successively formed, (still within the same time step) from the virtual displacement solutions (11) of equation (10). Similar equations would exist, in this example, for the other five independent components which contribute to the elements of the symmetric Hessian matrix. After all ten finite difference expressions corresponding to Equations (3), (10a→c), (12a→f) have been processed, the integrands of (4), (5), and (6) are formed for the current time step at specific positions corresponding to locations of receivers. These data are stored and the loop counter is then advanced one time step. This looping process continues until a set traveltime T_i is reached and the time integrations of (4), (5), and (6) can be completed.

From this illustration one can acquire a notion of how waveform tomography interrogates the independent material constants in reference to their individual contribution to the overall waveform under scrutiny. In this finite difference example, each cell of the numerical model would be allowed a distinct set of material parameters μ, λ_c, and ρ. Because of the heterogeneous formulation of the equations of motion (3), continuity conditions across cell boundaries are handled implicitly, allowing for consideration of very complex models. Only external boundaries (free surface and artificial model bounds at the bottom and sides) are handled explicitly. Because of the implicit internal boundary conditions, the finite difference method is a common method of choice for application to models with complex geometries.

In principle, the number of variable material parameters (three in the previous example) is not limited. A tomographic formulation for the eight independent material parameters of the Biot model can be similarly established. However, whether a stable, meaningful solution of the tomographic process for the full Biot model is achievable or not is very doubtful. A material constant hierarchy exists relative to significance of their effect on waveform shape and character. For the Biot model this

ordering has not yet been established. Least significant parameters would probably be masked by data and numerical tomographic process errors.

Application State of Waveform Tomography

Full waveform tomography, expressed in terms of nonlinear optimization, is not limited in application to particular data acquisition geometries. The process, in principal, can be applied to surface reflection, VSP, crosswell, and surface wave data. In the literature, however, applications appear only for the inversion of global surface wave data (Nolet 1987b) and for inversion of multi-offset seismic reflection data (e.g., Bamberger et al. 1982; Lines and Tritel 1984; Tarantola 1984, 1986, 1987; Gauthier Tarantola, and Virieux 1986; McAulay 1985; Kolb, Collino, and Lailly 1986; Mora 1987, 1988; Pan, Phinney, and Odom 1988; Pan and Phinney 1989; Helgesen and Kolb 1989; Cao et al. 1990; Pica, Tarantola, and Diet 1990; Sen and Stoffa 1991; Symes and Carazzone 1991; Bunks et al. 1995). References to the crosswell problem and VSP have not been found.

For waveform tomography, considerable preprocessing of data is required. The preprocessing steps are: (1) source specification, (2) source radiation correction, (3) attenuation correction, (4) muting and windowing, (5) wavelet deconvolution, and (6) two-and-a-half dimensional (2.5-D) corrections. Preprocessing procedures are given by Tura et al. (1992).

Most iterative full waveform inversion methods have been unsuccessful at inverting seismic data obtained from complicated models. The primary difficulty is the presence of numerous local minima in the objective function $F(\mathbf{p})$. The presence of local minima at all scales in the seismic inversion problem prevent iterative methods of inversion from attaining a reasonable degree of convergence to the neighborhood of the global minimum (absolute minimum of $F(\mathbf{p})$). In addition, when an initial parameter model gives rise to large kinematic errors between observed and modeled data, a perturbation of the parameter model has no effect on the value of the objective function, and consequently the gradient, $\mathbf{g}(\mathbf{p})$, is zero without being at the global minimum. The solution to both of these problems is to choose an initial parameter distribution which is close to the global minimum. Obviously, this answer is not the answer, since the global minimum is the solution that we seek. But the problem of convergence to the global minima is the subject of intensive current research (e.g., Bunk 1995).

At this time, waveform tomography is more of an art form than a robust, user friendly process. Most researchers are still trying to overcoming the local minimum problem for simply velocity models. Mora (1987), and Sen and Stoffa (1991) have extended their studies to simultaneous inversion for both velocity and density, while Cao et al. (1990) have simultaneously extracted velocity and impedance. But it is obvious that we are still at the threshold of routine waveform tomographic applications, and certainly not close to consideration of multiparameter Biot models. While the process machinery is essentially in place, the road map for routine convergence to the global minimum is not.

Diffraction Tomography

Concept Formulation

For crosswell, full wave imaging, diffraction tomography appears to be the method of choice. This method uses transmitted, reflected, and diffracted events to provide information relative to material parameter distribution within a panel bounded by two boreholes. The method also has been applied to VSP data.

The basic principle of diffraction tomography is simple. Consider a wave incident on an object in a homogeneous, infinite medium. For simplicity, consider the case of the acoustic wave equation with constant density. The object is described by the velocity distribution $C(\mathbf{r})$, where $\mathbf{r}$ is the position vector. The host medium has a velocity C_0. The wave equation in the source-free region is

$$\nabla^2 u(\mathbf{r}) + \frac{\omega^2}{C^2(\mathbf{r})} u(\mathbf{r}) = 0, \tag{13}$$

where $u(\mathbf{r})$ is a scalar quantity of the field such as pressure, ω is the angular frequency, and ∇^2 is the Laplacian operator.

Define the object function $O(\mathbf{r})$ as

$$O(\mathbf{r}) = 1 - \frac{C_0^2}{C^2(\mathbf{r})}, \tag{14}$$

and substitute into (13) to obtain

$$\nabla^2 u(\mathbf{r}) + k^2 u(\mathbf{r}) = k^2 O(\mathbf{r}) u(\mathbf{r}), \tag{15}$$

where $k = \omega / C_0$ is the wavenumber of the field in the host medium. Let

$$u(\mathbf{r}) = u^0(\mathbf{r}) + U(\mathbf{r}), \tag{16}$$

where $u^0(\mathbf{r})$ is the incident wave and $U(\mathbf{r})$ is the scattered wave. Substituting into (15), we have

$$\nabla^2 U(\mathbf{r}) + k^2 U(\mathbf{r}) = k^2 O(\mathbf{r}) u(\mathbf{r}). \tag{17}$$

By using the free-space Green's function $G(|\mathbf{r} - \mathbf{r}'|)$, we obtain

$$U(\mathbf{r}) = -\int_V k^2 O(\mathbf{r}')u(\mathbf{r}')G(|\mathbf{r}-\mathbf{r}'|)d\mathbf{r}', \tag{18}$$

where the integration is taken over the volume of the object. Assuming the object is a weak inhomogeneity, the Born approximation $\left(u \approx u^0\right)$ applies and (18) becomes

$$U(\mathbf{r}) = -\int_V k^2 O(\mathbf{r}')G(|\mathbf{r}-\mathbf{r}'|)u^0(\mathbf{r}')d\mathbf{r}'. \tag{19}$$

Within this formulation the anomalous velocity variations, as expressed by $O(\mathbf{r})$, form a basis for virtual sources impressed on an otherwise homogeneous medium of constant velocity C_0. These virtual sources result in a scattered field $U(\mathbf{r})$. Diffraction tomography involves the inversion of (19) for the velocity distribution $O(\mathbf{r})$ in terms of $U(\mathbf{r})$. This inversion is accomplished by initially assuming that the incident energy is a plane wave, and that the receiver is sufficiently removed from the scattering objects that the scattered wave may be considered plane also. These assumptions, together with the Fraunhofer approximation for the Green's function, allows the scattered plane wave in a given direction to be found from the 3-D Fourier transform of the object function (e.g., Devaney 1984). Theory can be expanded to include multiple point sources (Harris 1987) for reflection, crosswell, and VSP applications (Wu and Toksöz 1987). The problem of uniform medium assumption has been addressed by Devaney and Zhang (1991), Dickens (1994), Gelius (1991, 1995a,b), and others.

Application State of Diffraction Tomography

Several workers have used synthetic data (Devaney 1982, 1984; Wu and Toksöz 1987; Lo, Duckworth, and Toksöz 1990) to demonstrate the ability of diffraction tomography to produce velocity images, with a spatial resolution of less than one wavelength, of isolated, weakly scattering targets embedded in a constant-velocity background. Others (Lo et al. 1988; Pratt and Worthington 1988) have used diffraction tomography to image low-contrast scale models, and the algorithm has also been applied to field data (Tura et al. 1992). These studies have used the filtered back-projection diffraction tomography algorithm (Devaney 1982, 1984; Wu and Toksöz 1987) which is applicable only for the case of weak scatterers in a constant-velocity medium. In general, these restrictions make it impossible to apply the traditional filtered back-propagation diffracted tomography algorithms to arbitrary models of realistic geological complexity.

Dickens (1994) applied diffraction tomography to the problem where the velocity structure can be approximated by a set of horizontal layers He shows that given an initial layered model that adequately represents the average structure of the subsurface, and an accurate calculation of the background wavefield propagating through this model, layered diffraction tomography can be used to successfully image complex, geologically

realistic models to which the traditional filtered back-propagation diffraction topography algorithm is inapplicable.

A generalized diffraction tomography algorithm, applicable for an arbitrary background structure, has been studied by Gelius et al. (1991), and Gelius (1995a,b). The method is valid for a two-dimensional nonuniform background model and point source illumination (i.e., a 2.5-dimensional geometry). This method is regarded as a generalization of the iterative algorithm of Ladas and Devaney (1991), which is valid only for line sources and two-dimensional homogeneous background models.

As in the case of waveform tomography, extensive preprocessing of field data is required. And, as in the former case, only first arrival waveform energies are generally considered. The necessity of assumption of weak scattereres in a constant-velocity medium eliminates traditional filtered back-projection diffraction algorithms for application consideration to the liquefaction problem. On the other hand, the diffraction algorithms of Gelius (1995b) look promising.

Categorically, diffraction tomography is based on the acoustic wave equation and has focused only on inversion for anomalous velocity distributions. There are inherent difficulties within the formulation that would be presented if density variations were also allowed. Thus, density is always assumed constant, and only first arrival P-wave energy waveforms are used in the formulation to obtain estimates of compressional wave velocity distributions.

Traveltime/Attenuation Tomography

Concept Formulation

Traveltime/attenuation tomography begins with establishing a cellular model, which dimensionally corresponds to a section of the real earth under investigation. Each cell of the model is a square (or triangle) in two-dimensions, or a cube (or tetrahedron) in three-dimensions. Associated with each cell is an assigned slowness, sij. Provisions must then be established for calculation of minimum traveltimes from source positions to receiver positions for waves traversing the cellular structure. For each source-receiver pair the minimum travel path must be superposed upon the cellular structure, and the path length segment must be calculated for each cell intercepted by the 'ray'. These path length segments form the matrix $\tilde{\mathbf{A}}$.

A common approach to traveltime/attenuation tomography begins with the basic equation

$$t_i = \sum_{j=1}^{N} A_{ij} s_j \qquad i = 1...M, \tag{20}$$

where t_i is the traveltime or amplitude associated with the i-th ray; A_{ij} the pathlength of the i-th ray in the j-th cell; and s_j is the slowness or absorption value of the j-th cell, or in matrix notation,

$$\mathbf{t} = \tilde{\mathbf{A}}\mathbf{s}. \tag{21}$$

When (21) is solved directly, the squared solution length is given by $\mathbf{s}^{\mathrm{T}}\mathbf{s}$, and constraints involving solution length seek a model with minimum overall parameter estimates. This is not desirable, and provides motivation for reformulating the problem in terms of a background model and perturbation values, exactly as is done when linearizing a nonlinear problem. Then the basic equation to solve is

$$\Delta\mathbf{t} = \tilde{\mathbf{A}}\Delta\mathbf{s}, \tag{22}$$

where $\Delta\mathbf{s} = \mathbf{s} - \mathbf{s}_0$, $\Delta\mathbf{t} = \mathbf{t} - \mathbf{t}_0$, and $\mathbf{t}_0$ are vectors of theoretical data values associated with the reference model $\mathbf{s}_0$. Any of several methods might be used to solve (22) for $\Delta\mathbf{s}$, including the direct or singular value decomposition (SVD) computed generalized inverse (Golub and Reinsch 1970; Lines and Treitel 1984; Lines and Lafehr 1989), back-projection methods such as ART (Tanabe 1971; Dines and Lytle 1979) or SIRT (Gilbert 1972; Ivansson 1986), sparse system conjugate gradient methods (Hestenes and Stiefel 1952; Paige and Saunders 1982; Scales, Gersztenkorn, and Treitel 1988), and composite distribution methods (Clippard, Christensen, and Rechtien 1995). For most tomography problems, $\tilde{\mathbf{A}}$ is ill-conditioned, and direct solution results in unstable model parameter estimates. To stabilize the solution, a priori information must be added. This information in usually specified in the form of auxiliary constraints implemented via weighting matrices. The objective function to be minimized is then given by

$$E = \left(\tilde{\mathbf{A}}\Delta\mathbf{s} - \Delta\mathbf{t}\right)^{\mathrm{T}} \tilde{\mathbf{W}}_e \left(\tilde{\mathbf{A}}\Delta\mathbf{s} - \Delta\mathbf{t}\right) + \Delta\mathbf{s}^{\mathrm{T}}\tilde{\mathbf{W}}_m\Delta\mathbf{s}, \tag{23}$$

where $\tilde{\mathbf{W}}_m$ and $\tilde{\mathbf{W}}_e$ are model and error weighting matrices, respectively. If we define $\tilde{\mathbf{W}}_m \equiv \tilde{\mathbf{D}}_m^{\mathrm{T}}\tilde{\mathbf{D}}_{\mathrm{m}}$ and $\tilde{\mathbf{W}}_e \equiv \tilde{\mathbf{D}}_e^{\mathrm{T}}\tilde{\mathbf{D}}_e$, then an L_2 penalty function interpretation of E is

$$E = \left\| \begin{bmatrix} \tilde{\mathbf{D}}_{\mathrm{e}} & \tilde{\mathbf{A}} \\ \tilde{\mathbf{D}}_{\mathrm{m}} & \tilde{\mathbf{I}} \end{bmatrix} \Delta\mathbf{s} - \begin{bmatrix} \tilde{\mathbf{D}}_{\mathrm{e}}\Delta\mathbf{t} \\ \mathbf{0} \end{bmatrix} \right\|_2 . \tag{24}$$

The weighted least-squares parameter estimates may be written as

$$\Delta\mathbf{s} = \left(\tilde{\mathbf{A}}^{\mathrm{T}}\tilde{\mathbf{D}}_e^{\mathrm{T}}\tilde{\mathbf{D}}_e\tilde{\mathbf{A}} + \tilde{\mathbf{D}}_m^{\mathrm{T}}\tilde{\mathbf{D}}_{\mathrm{m}}\right)^{-1} \tilde{\mathbf{A}}^{\mathrm{T}}\tilde{\mathbf{D}}_e^{\mathrm{T}}\tilde{\mathbf{D}}_e\Delta\mathbf{t}. \tag{25}$$

The success of this inversion process, yielding corrections $\Delta \mathbf{s}$ to the background slowness $\mathbf{s}_0$, depends upon the accuracy of the elements of $\tilde{\mathbf{A}}$, which in turn depend upon the method used to calculate minimum traveltimes. Traveltimes may be obtained by direct (numerical) or indirect (ray tracing) solution of the eikonal equation (see Cerveny and Hron 1980). The only field variable required to solve the eikonal equation is the propagation velocity, but direct efficient numerical solution of the eikonal equation is difficult when the velocity field is complicated. Thus, many traveltime applications involve ray-tracing methods. Ray-tracing equations are ordinary differential equations derived by applying the method of characteristics to the eikonal equation (Cerveny and Hron 1980). The ray equations may be solved with shooting methods, which pose ray tracing as an initial value problem, or with bending methods, which pose ray tracing as a two-point boundary value problem.

Alternately, other direct numerical solutions of the eikonal equation are possible. Vidale (1990) succeeded with a finite difference scheme that makes a plane-wave approximation. A similar approach was taken by Podvin and Lecomte (1991). Moser (1991) presents a graph theory approach; Schneider et al. (1992), a Fermat's principle approach; van Trier and Symes (!991), a two-dimensional upwind finite difference approach; and Schneider (1995), a three-dimensional upwind finite difference solution of the eikonal equation.

Application State of Traveltime/Attenuation Tomography

First arrival tomographic algorithms, far too many to list, have proven to be quite useful for delineating subsurface structure. Most of these algorithms are two-dimensional, limiting imaging to a panel defined (generally) by two vertical boreholes. In every case it is the first arrival within a seismic trace that is used for input data. Thus, methods to date have considered only compressional wave energy.

High resolution inversion requires that the number of cells (pixels) within the image section be less than or equal to the number of independent traveltime (or amplitude) measurements. By independence it is implied, for example, that two closely spaced parallel rays traversing the same cells would only count as a single measurement. Thus, the available number of independent traveltime measurements determines the size of the image cell, and, consequently, spatial image resolution. However, if one does not require high resolution of image parameters (via optimum minimization of the objective function), but rather desires a more detailed relative distribution image (not too accurate in the values of the imaged quantity), then the cell size can be made smaller, and iterative back-projection methods such as ART or SIRT can be used. Examples of the latter technique is given by Rechtien and Ballard (1993).

Hybrid Tomography

Biot Theory Applications

Yamamoto, Nye, and Kuru (1994) introduced a procedure to extract the material properties of unlithified sediments such as porosity, permeability, and shear strength directly from crosswell compressional wave velocity images. The Biot (1956a) theory and an empirical relation (Yamamoto et al. 1989) between porosity and shear modulus were used to extract the porosity images and the shear strength images from the velocity images. This procedure was successfully applied to an alluvial sediment strata in Tokyo Bay. Yamamoto, Nye, and Kuru (1995), extended the application of this procedure to the case of mixed lithified and unlithified sediments comprising a Florida limestone aquifer. They adapted the unified BISQ flow theory in Dvorkin and Nur (1993), Dvorkin, Nolen-Hoeksema, and Nur (1994), and Dvorkin, Mavko, and Nur (1995) for extraction of permeability, and the empirical model in Han, Nur, and Morgan (1986) for extraction of porosity and shear strength.

Application state of hybrid tomography

The results of Yamamoto, Nye, and Kuru (1994) for the unlithified sediment in Tokyo Bay are impressive for the extraction of porosity and shear strength images from compressional wave crosswell data. The extraction of a permeability image was less successful due to non-observance of clear velocity-frequency dispersion within the experimental frequency range (1 kHz - 10 kHz). These results were based on the adoption of the Biot low-frequency theory as an adequate unlithified sediment (alluvial clays and sands) model.

The results of Yamamoto, Nye, and Kuru (1995) were for a mixed lithified and unlithified sediment. In this experiment, porosity and shear velocity estimations were based upon a specific empirical model of a lithified sediment, as given by Han, Nur, and Morgan (1986). This model first relates porosity to compressional wave speed (as given by velocity imaging of first arrival field data) and a measure of clay content (measured or assumed). Secondly, shear wave velocity is expressed in terms of porosity (as calculated in the first step) and clay content. Shear strength is then calculated by using assumed, or measured, values of grain and pore fluid densities. These calculations can be performed for low-frequency compressional wavefield data providing a low-frequency empirical lithified sediment model is established.

Permeability was estimated by fitting the velocity -frequency dispersion data of the Biot (1956) model or the BISQ model (Dvorkin, Nolen-Hoeksema, and Nur 1994) with corresponding field data extractions. Experimentally, Yamamoto, Nye, and Nur (1994, 1995) employed an acoustic pulse with its energy concentrated near a certain frequency by using a narrow-band pseudo random binary sequence code as a source signal. Crosswell measurements through the same cross-section were repeated many times using different frequencies ranging from 200 to 5000

Hz. The inhomogeneous structure of rock permeability was indicated by images obtained by taking differences of velocity images acquired at different carrier frequencies.

Non-Tomographic Seismic Methods

Empirical methods have been developed to evaluate liquefaction resistance directly from shear wave velocity (Bierschwale and Stokoe 1984). Conventional crosswell (non-imaging) and downhole shear wave methods have been employed (Stokoe and Hoar 1978; Woods 1978; Sirles 1987) to obtain depth estimates of shear wave velocity. Nazarian and Stokoe (1984) developed the Spectral Analysis of Surface Waves (SASW) procedure, where the distribution of shear wave velocity with depth is determined by phase velocity analysis of Rayleigh waves. Sirles (1987) investigated liquefaction in terms of amplitude attenuation of shear waves in a crosswell experiment. These methods are all, essentially, one-dimensional in that they give variation of shear waves with depth only along a vertical line arbitrarily positioned at the midpoint of the two measurement points. Basically, the fundamental assumption common to all these methods is that the local earth is composed of uniform horizontal layers. Some semblance of lateral variation of shear velocity can be obtained by shifting the experimental arrangement (whether boreholes are surface instrumentation) laterally and collecting a suite of data along a horizontal profile. But these methods are not, in any true sense, two-dimensional as are the tomographic methods previously discussed. Nevertheless, these methods have produced shear wave velocity estimates useful to the liquefaction problem.

Compressional and shear wave refraction methods are also occasionally applied. However, the hidden layer problem (low velocity layer beneath a high velocity layer) presents a very real and commonly encountered pitfall that often renders refraction profile data meaningless. Worse yet, the presence of this condition is difficult to detect and usually must be determined by some other means.

Since these conventional methods are familiar to investigators in the field of liquefaction, no further discussion of them will be made. The interested reader can refer to the references cited.

5 Conceptual Field Tests

Potential Seismic Methods for Liquefaction Studies

Shear waves are the dominant energy fields used for the assessment of liquefaction potential. Shear wave velocity, by virtue of its relation to the shear modulus, is an indicator that is directly linked to the development of pore water pressure in soils under cyclic loading. However, since shear wave energy is never the first arrival in a seismic trace, even though shear sources and cross-polarized acquisition procedures are employed, it is extremely difficult to achieve high accuracy in measurement of arrival time of shear waves. The error in arrival time is considerably greater than that for first arrival compressional energy, and, consequently, substantial error in shear wave velocity results.

To my knowledge, traveltime tomography has never been applied (in the classical sense) to the problem of direct extraction of shear velocity distributions. But it is possible, in principal, to directly extract shear wave information by use of waveform tomography. So we are faced with the dilemma that procedural problems for the latter must still be worked out to make the method useful, and the former method works well for compressional waves, but not shear. Thus, at this time, it seems that we are left with conventional methods, as discussed in the previous section, and compressional wave traveltime/attenuation tomography to investigate the liquefaction problem.

Traveltime/attenuation tomography for first-arrival compressional wave energy is useful for the study of liquefaction for several reasons. First, tomographic compressional wave velocity images yield information relative to overall fabric and structure of the medium. Secondly, attenuation tomography provides spatial distribution of overall (all frequencies) material attenuation. Frequency dependent attenuation, or, equivalently, the quality factor Q, can possibly be obtained by imaging narrow-band filtered first arrival amplitudes. Thirdly, shear wave velocity and porosity distributions can be derived from compressional wave traveltime/attenuation tomographic data by application of the empirical method of Yamamoto, Nye, and Kuru (1994). Depending on signal bandwidth, permeability estimates might also be obtained from compressional wave data by means of the empirical method.

Compressional wave tomography can be used in conjunction with conventional procedures. Spectral analysis of surface waves (SASW) can be conducted independent of any tomographic data gathering activity. This method results in estimation of shear wave velocity with depth. In addition, crosswell and downhole shear wave studies can be made using the same boreholes employed for tomographic studies. SASW, conventional crosswell and downhole shear wave studies are, essentially, one-dimensional in that velocity is assumed laterally constant, but variable with depth. Thus, tomography is here proposed as a supplemental procedure to conventional one-dimensional methods.

Although currently constrained by inadequacy of data processing procedures, waveform tomography remains the imaging goal. The advent of adequacy is, perhaps, near future, and it seems reasonable to execute appropriate data gathering procedures that would render data suitable for future analysis by advanced methods. Consequently, in addition to conventional SASW, crosswell, and downhole shear wave studies, I propose the following data acquisition procedures:

1) Combined crosswell & borehole-to-surface (CCBS), full waveform data gathering, using compressional wave sources and hydrophones.

2) Combined crosswell & borehole-to-surface (CCBS), full waveform data gathering, using clamped shear wave sources and clamped three-component seismometers.

3) Full waveform Rayleigh wave (FRW) study using a vertical surface impact source, eighteen three-component surface seismometers, and two three-component clamped borehole seismometers.

4) Full waveform Love wave (FLW) study using a horizontal surface impact source, eighteen three-component surface seismometers, and two three-component clamped borehole seismometers.

Experimental Geometry - CCBS

Field Configuration

Figure 1 shows the proposed experimental arrangement. Assume a zone of anomalous wave velocity, density, porosity, permeability, etc. embedded in a typical soil environment. We make no assumption of material distributions, water saturation, water table depth, etc..

A system of four boreholes is desirable, although two would suffice. Each borehole consists of a 4 inch-diameter (minimum) PVC pipe. This pipe must be appropriately grouted to the host medium. The depth of each borehole will be approximately three times the anticipated depth of the anticipated liquefiable zone (3D). The horizontal spacing of these holes

will be approximately one-third the anticipated depth of the zone (D/3). In the event of having only two boreholes, the desired borehole spacing would be (D). These boreholes must be sealed in order to enable the

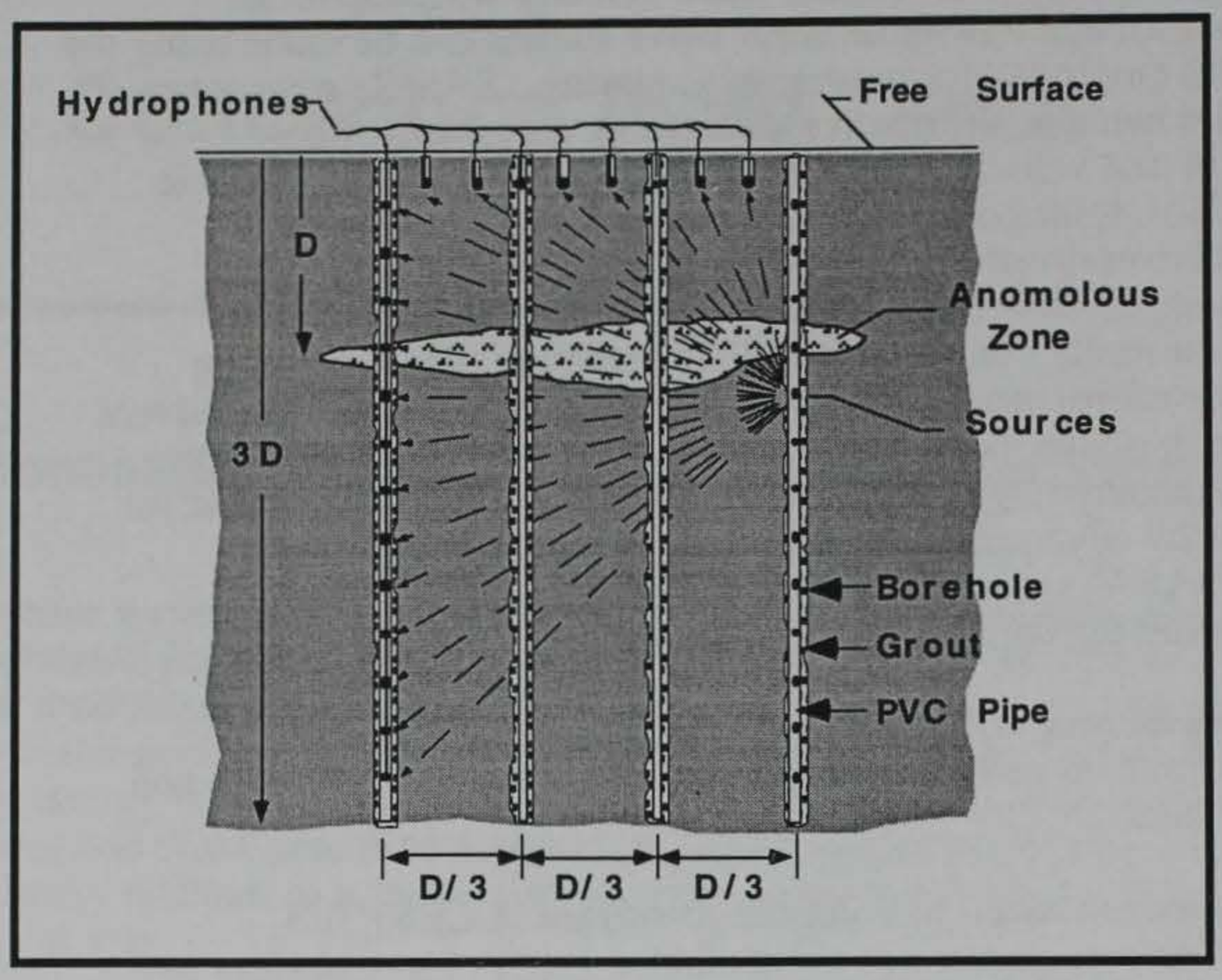

Figure 1. Common source acquisition configuration for tomography.

maintenance of a full column of water in each PVC pipe. In addition, shallow holes, approximately two feet in depth, will be emplaced along the profile. These holes will be lined with plastic to enable the maintenance of a shallow water column.

Two separate data sets will be gathered. The first set, as illustrated in Figure 1, will employ broad band hydrophones as the sensing elements and a high-frequency sparker system as the energy source. This system is designated as the Borehole Imaging and Tomographic System (BITS), a product of past Waterways Experiment Station (WES) tomographic research. A description of BITS can be found in Rechtien, Hambacker, and Ballard (1993). The second data set will be gathered by the use of wall-clamped three-component geophones, surface three-component geophones, and a wall-clamped vertical polarizing shear wave source.

For the collection of data suitable for waveform tomography (having in mind future data processing capability), it is necessary that all receiving instrumentation have similar dynamic response. Consequently, it is not permissible to mix instrumentation; i.e., borehole hydrophones and surface geophones.

During acquisition of both sets of data, source locations will be established in one of the outer boreholes and receiver locations established in the other outer borehole and along the ground surface between these two boreholes. As indicated in Figure 1, seismic energy generated at a given source position will be recorded (non-simultaneously) at selected receiver

positions. The acquisition procedure employed is designed to acquire maximum density of ray coverage in the upper two-thirds of the vertical panel defined by the outer two boreholes.

The inner two boreholes, separated by a spacing of D/3, shall be used for the collection of conventional crosswell and downhole shear wave data for comparison with tomographic shear velocity images.

BITS Instrumentation

The BITS system records data within the frequency bandwidth of 10 Hz to 2 kHz (an anti-alias filter is set at 2 kHz). The signal bandwidth dictates the spacing of instrumentation on the surface and within the borehole. Within the borehole, hydrophones will sense tube waves superposed upon

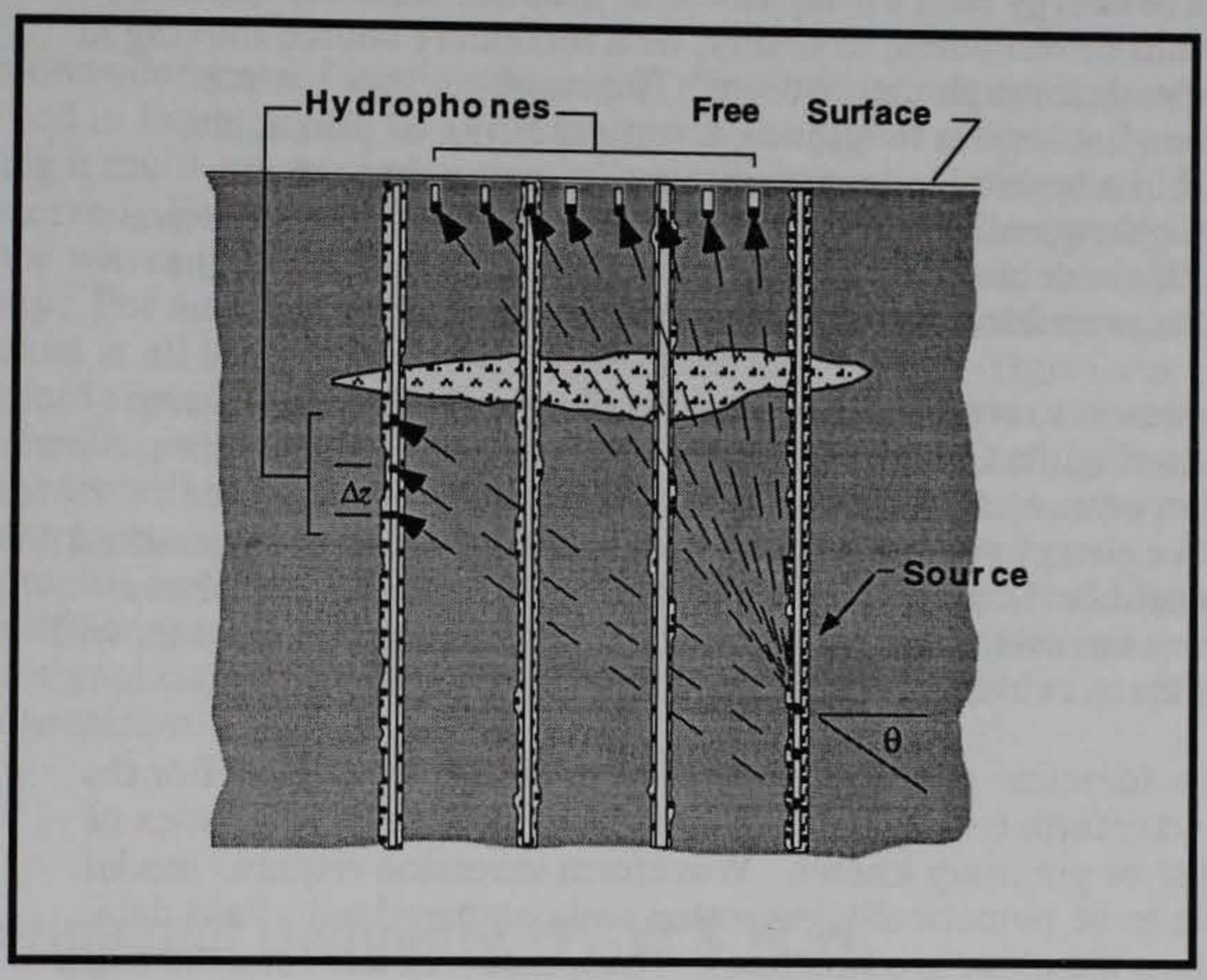

Figure 2. Constant vertical offset data gathering configuration. A single hydrophone and a single source, vertically offset by an angle θ, are simultaneously raised a distance Δz between data acquisition cycles. Fixed surface hydrophones are sampled for every source position.

desired crosswell body wave transmissions. Tube waves are generated primarily by the very process of source wavefield incidence upon the borehole. A second tube wave effect occurs in the data as a result of tube wave conversion within the source borehole, with the converted waves acting as secondary sources. By employing a constant vertical offset data collection procedure, where both source and receiver, vertically separated by a given, fixed distance, are simultaneously raised to shallower positions between recordings (see Figure 2), both tube wave effects are manifested within the constant vertical offset trace record as events falling along a line with inverse slope approximately equal to the tube wave velocity. These effect can be readily removed from the data by used of frequency-

wavenumber velocity filters provided the data is not spatially aliased. Spatial aliasing occurs when,

$$\Delta z < \frac{V_t}{4 f_{\max}}, \tag{26}$$

where Δz is the sensor spacing, V_t is the tube wave velocity, and $f_{\max}$ is the maximum frequency with non-trivial signal strength. The tube wave velocity is in the neighborhood of 4000 fps, given a water-filled borehole. Thus for borehole hydrophones, and a maximum frequency of 2 kHz, both source and hydrophone station spacing should be 0.5 ft or less.

A third tube wave effect to consider is that the tube wave velocity might exceed the compressional wave velocity in the cohesionless soil. While tube wave energy falls off rapidly with distance from the center of the tube, it would nevertheless, in reality, be a secondary source moving at 'supersonic' speeds through the medium. The resulting shock wave process is somewhat similar to igniting a vertical string of primacord suspended within a borehole, or to an airplane plowing through the atmosphere. Consequently, it is necessary to use mechanical tube wave attenuators both above and below the source and above and below the receiver. These attenuators are commercially available.

A second reason to employ tube wave attenuators is that tube wave energy encountering the free surface is not only partially reflected, but significant tube wave energy is converted to body and surface waves. Since tube wave energy will arrive at the surface in advance of transmitted body waves, converted energy might be recorded at surface hydrophone positions as first arrivals. Consequently, the desired transmitted events will be masked by these converted waves.

A final consideration concerns estimation of source signature. For the execution of waveform tomographic data processing the characteristics of the source must be precisely known. Waveform inversion requires model waveform data to be numerically generated and compared with field data (specified within the objective function). Thus, modeled data must contain not only the complex spectral content of the source, but also the spatial radiation pattern effects of source and receiver borehole coupling. From the viewpoint of modeling, the boreholes don't exist; only point sources and point receivers buried within the medium.

Source characteristics can generally be gleaned from the set of first arrival waveforms. These waveforms include the effects of source spectral content, source radiation and receiver reception patterns, and signal modification along the transmission path. The source spectral content can be continually monitored by a spatially fixed hydrophone mounted within, and near the top of, the source borehole. Consequently, source spectral variations can be corrected from these monitored signals. Sets of constant vertical offset crosswell data yield information relative to source radiation and receiver reception at various ray angles. Long wavelength filtering of these data will remove effects of spatially small material inhomogenities in the data, thus bringing clarity to source radiation and receiver reception geometries. Finally, attenuation tomography clearly shows borehole

coupling problems due to inadequate grouting between the PVC pipe and host medium. Amplitude and traveltime corrections to affected traces in the total data set will remove these undesirable tomographic anomalies.

Shear Instrumentation

For the emplacement of wall-clamped instrumentation, the borehole can be air-filled. While tube waves still exist in and around an air-filled borehole, the magnitude of such energy is not significant. Acoustic mufflers above and below the instrumentation will suffice to remove any tube wave problem. However, spatial filtering of the data may still be required in order to arrive at definition of source radiation and receiver reception patterns (as discussed in the previous paragraph on BITS instrumentation). Therefore, precautions must be taken to insure that the data is not spatially aliased.

In consideration of spatial aliasing in the previous section, the velocity specified in Equation (26) was referred to as the tube wave velocity. When viewing a multi-trace seismogram, a linear alignment of energy can often be observed. For water-filled borehole data, the obvious energy alignments are tube waves. The inverse slopes of these alignments yield the tube wave velocity. For air-filled boreholes tube waves should not be observable. If they exist at all their velocity would be close to 1100 fps. Thus for a maximum signal frequency of, say, 200 Hz, Equation (26) would require instrumentation spacing of about 1.3 ft. Although it is doubtful that such alignments will be observable in air-filled borehole data, it must be recalled that instrumentation spacing also determines the pixel size of the tomographic image. Consequently, a spacing of 1 to 1.5 ft would be most desirable for shear wave data gathering. Previous comments concerning source signal estimation for hydrophones is equally applicable for clamped instrumentation.

Experimental Geometry - FRW & FLW

Field Configuration

Employing a 48 channel recording system, 18 stations will be established along the dam, with the borehole configuration near the center of the spread. Station spacing will be in the neighborhood of 5 feet. A three-component seismometer will be installed at each station.

Simultaneously employing an additional 6 channel recording system, two three-component clamped geophones will be installed at depths of D and 2D within a single borehole.

For the Rayleigh wave study (FRW), energy will be supplied alternately at both ends of the line by means of a vertical hammer blow upon a plate. For the Love wave study (FLW), energy will be supplied by alternately striking both ends of a vertically loaded wooden beam with steel

end caps. The beam will be oriented with long axis horizontal and perpendicular to the instrumentation line.

In the process of waveform tomography the modeled wave field is generated. Such wave fields include waveforms at depth. Consequently, having borehole measurements of the shallower roots of both Rayleigh and Love waves provides a means of assessing the accuracy of the tomographic process.

Conventional Seismic Tests

The inner two boreholes of Figure 1 are for conventional downhole and crosswell testing (Butler and Curro, 1981). Crosswell testing involves horizontal transmission paths only, and employs clamped, vertical polarized shear sources and three-component wall-clamped geophones. Downhole testing involves surface SH cross-polarized sources and three-component wall-clamped geophones.

The primary reason for the additional two boreholes is that tomographic images are least accurate near instrumentation boreholes. The reason for lack of accuracy is the convergence of all source-receiver raypaths to single points at the borehole rather then having rays more uniformly spread out within the pixel, as they are in regions more central to the image. Thus image data is, supposedly, more accurate in the central regions of the tomograph, and probably more correlatable to conventional shear wave estimates. However, this is a minor point, and confinement to two boreholes, instead of four is satisfactory provided the borehole spacing D is small enough to avoid lack of signal strength.

In the event that the two inner boreholes are not available, no additional data gathering is required for conventional crosswell and downhole procedures. Conventional crosswell and downhole data is included within the tomographic data sets.

No additional data gathering is required for the SASW procedure. Spectral analysis of surface waves can be conducted between any two stations of the FRW data set. Thus, numerous pairs of surface measurements, with a variety of station spacing, will be available for spectral analysis.

6 Summary

The BISQ theory is acceptable as a theoretical dynamic model of unlithified, or partially lithified, saturated, or partially saturated, soil when subjected to low amplitude seismic wave energy. Finite difference numerical modeling methods exists for calculation of synthetic wave fields within a heterogeneous Biot solid. Extension to the BISQ solid is straightforward. Compressional, shear, and fluid wave components are incorporated within the formulation. Existing computer algorithms can be expanded for three-dimensional geometries.

Full-waveform tomographic methods are potentially applicable to Biot and BISQ solids. Potential exists for simultaneous inversion of multiple model parameters. But problems concerning convergence of the objective function to the global minimum have not yet been fully resolved. Consequently, full-waveform tomography, while certainly the most desirable tomographic application, is not yet on-line as a routine inversion method.

Diffraction tomography is based on the acoustic wave equation and is focused only on inversion for anomalous velocity distributions. Inherent difficulties within the formulation would be presented if density variations were also allowed. The method is applicable only to weak scatterers in a medium of constant background velocity. Some movement of the theory has been made toward application to an arbitrary background structure. In its present form if offers no advantage over traveltime tomography, and, henceforth, should not be seriously considered as a potential method applicable to the liquefaction problem.

Traveltime/attenuation tomography is fully developed. Inversion of first-arrival traveltime data yields spatial estimates of a quantity called 'velocity'. This quantity can be correlated with the spatially variable material velocity only if realistic transmission paths are employed within the forward model calculation of the inversion process. The use of straight raypath tomographic algorithms, for example, can never yield correct velocity estimates within a spatially limited low velocity zone. Curved raypath and wavefront algorithms yield better, but not totally accurate, results. Inversion of first-arrival amplitudes yields estimates of a spatially distributed quantity call 'attenuation'. This quantity, however, has no direct correlation to fundamental model parameters (i.e., frame or fluid

viscosity, etc.). Attenuation images only reveal zones of overall, broad-band energy diminution.

The hybrid tomographic method of Yamamoto, Nye, and Kuru (1994) define porosity and shear velocity as image parameters. Estimates of these parameters are derived from compressional wave crosswell data. These estimates are based upon empirical relationships derived from Biot's low-frequency theory. While their results are interesting, correlation with independent estimates of porosity and shear velocity must be made for validation.

It is taken for granted that the exhaustive seismic response of a liquefiable, cohesionless soil can be fully captured within appropriate field measurements of seismic waves. Instrumentation and field procedures are sufficiently developed for accurate, comprehensive acquisition of seismic data. The potential for data quality far exceeds current ability to extract liquefiable-relevant material parameters from recorded seismic waveforms. Nevertheless, it is expedient to collect data in anticipation of resolution of current inversion limitations.

Currently, direct extraction of material parameters from a tomographic seismic data set is limited to compressional wave velocity and attenuation. Shear wave velocity may also possibly be directly extracted, given sufficient angularity of borehole shear source radiation strength and ability to separate out compressional energy arrivals. Empirical procedures allow the expression of shear wave strength and porosity from compressional wave data. Permeability estimates may possibly be empirically derived, given sufficient data bandwidth. Compressional wave tomographs also yield information relative to soil fabric and structure.

Surface wave studies will generate data suitable for future waveform tomography. Currently, however, conventional SASW techniques can be applied to both Rayleigh and Love wave data sets (a SASW procedure for Love waves is probably available somewhere).

Conventional crosswell and downhole shear wave tests are well established.

7 Conclusion

An existing, limited data set suggest that shear wave velocity may be a useful index of liquefaction potential (Finn 1995a). Shear wave velocity is influenced by many of the variables that influence liquefaction, such as, soil density, confinement, stress history and geologic age. The major advantage of using shear wave velocity as an index of liquefaction resistance is that it can be measured in soils that are hard to sample, such as cohesionless silt, sand, or hard to penetrate gravel.

Currently, seismic methods applied to the problem of in situ determination of liquefaction potential of cohesionless soils are limited to the determination of shear wave velocity. Conventional crosswell, downhole, seismic cone penetrometer, and SASW surface wave methods are the primary seismic tools employed. These methods are one-dimensional, yielding, effectively, velocity values for a vertical sequence of horizontal 'layers' of arbitrarily chosen thickness.

Any seismic field method that could increase the accuracy of measured shear wave velocity, or expand velocity estimation to two or even three dimensions would be most valuable. Moreover, seismic methods that could produce estimates of other material parameters, such as density, porosity, permeability, frame or fluid viscosity, etc., would be extremely welcomed.

Waveform tomography holds the promise of expansion of the seismic liquefaction index beyond shear wave velocity. Currently, waveform tomography has been applied to the simultaneous evaluation of velocity and density for an acoustic medium (Mora 1987; Sen and Stoffa 1991). While problems are unresolved relative to minimization of the objective function of inversion procedures, the potential for multi-parameter estimation for even the BISQ model is promising.

Field tests proposed within the body of this report have in view advanced data processing capability. Two-dimensional, crosswell, tomographic data gathering exercises are proposed. These experiments include borehole-to-surface measurements for the purpose of imaging shallow targets. In addition, two-dimensional, surface wave experiments are proposed. One exercise will be conducted for collection of Rayleigh wave data, and one for the recording of Love waves.

While awaiting resolution of full waveform tomographic inversion problems, traveltime attenuation tomography will be applied to measured crosswell measurements (including borehole-to-surface data). Tomographic results should give two-dimensional distribution estimates of compressional wave velocity and attenuation, soil fabric and structure, shear wave velocity, porosity, and possibly permeability. The last three items will be extracted from compressional wave traveltime and amplitude data by means of empirical relations (e.g., Yamamoto 1994).

It is experimentally feasible at this time to acquire data suitable for full waveform, multi-parameter tomography.

References

Badiey, M., and Yamamoto, T. (1985). "Inversion of normal incidence seismograms," *Geophysics*, 47, 757-770.

Biot, M.A. (1941). "General theory of three-dimensional consolidation," *J. Appl. Phy.* 12, 155-164.

____ (1956a). "Theory of propagation of elastic waves in a fluid-saturated porous solid, part I: Low-frequency range," *J. Acoust. Soc. Am.*, 28, 168-178.

____ (1956b). "Theory of propagation of elastic waves in a fluid-saturated porous solid, Part II: Higher frequency range," *J. Acoust. Soc. Am.*, 28, 179-191.

____ (1956c). "General solutions of the equations of elasticity and consolidation for a porous material," *J. Appl. Mech.*, 78, 91-96.

____ (1962a). "Mechanics of deformation and acoustic propagation in porous media," *J. Appl Phy.*, 33, 1482-1498.

____ (1962b). "Generalized theory of acoustic propagation in porous dissipative media," *J. Acoust. Soc. Am.*, 34, 1254-1264.

Bierschwale, J.G., and Stokoe, K.H. (1984). "Analytical evaluation of liquefaction potential of sands subjected to the 1981 Westmorland earthquake," Geotech. Engr. Report GR-84-15, Civ. Engr. Dept, U. of Texas, Austin.

Bunks, C., Saleck, F. M., Zaleski, S., and Chavent, G. (1995). "Multiscale seismic waveform inversion," *Geophysics*, 60, 1457-1473.

Burridge, R., and Keller, J.B. (1981). "Poroelasticity equations derived from microstructure," *J. Acoust. Soc. Am.*, 70, 1140-1146.

Butler, D. K., and Curro, J. R. (1981). "Crosshole seismic testing - Procedures and pitfalls," *Geophysics*, 46, 23-29.

CAEE (1995). "The Hyogo-ken-Nanbu (Kobe) earthquake of 17 January (1995)," Preliminary Reconnaissance Report, Canadian Assn. for Earthq. Engr., Vancouver.

Cerveny, V., and Hron, F. (1980). "The ray series method and dynamic ray-tracing sytem for three-dimensional inhomogeneous media," *Bull. Seis. Soc. Am.*, 70, 47-77.

Clippard, J.D., Christensen, D.H., and Rechtien, R.D. (1995). "Composite distribution inversion applied to crosshole tomography," *Geophysics*, 60, 1218-1294).

Coa, D., Beydoun, W., Singh, S., and Tarantola, A. (1990). "Simultaneous inversion for background velocity and impedance maps," *Geophysics*, 55, 458-469.

Dai, N., Vafidis, A., and Kanasewich, E.R. (1995). "Wave propagation in heterogeneous, porous media: A velocity-stress, finite difference method," *Geophysics*, 60, 327-340.

Devaney, A.J. (1982). "A filtered back-propagation algorithm for diffraction tomography," *Ultrasonic Imag.*, 4, 336-350.

____ (1984). "Geophysical diffraction tomography," *IEEE Trans. Geosci. Remote Sensing,* GE-22, 3-13.

Devaney, A.J., and Zhang, D.H. (1991). "Geophysical diffraction tomography in a layered background," *Wave Motion*, 14, 243-265.

Dickens, T.A. (1994). "Diffraction tomography for crosswell imaging of nearly layered models," *Geophysics*, 59, 694-706.

Dines, K.A., and Lytle, R.J. (1979). "Computerized geophysical tomography, " *Proc. IEEE,* 67, 1065-1073.

Dvorkin, J., and Nur, A. (1993). "Dynamic poroelasticity: A unified model with the squirt and the Biot mechanism," *Geophysics*, 58, 524-533.

Dvorkin, J., Nolen-Hoeksema, R., and Nur, A. (1994). "The squirt flow mechanism: Macroscopic description," *Geophysics*, 59, 428-438.

Dvorkin, J., Mavko, G., and Nur, A. (1995). "Squirt flow in fully saturated rocks," *Geophysics*, 60, 97-107

Domenico, S.N. (1974). "Effect of water saturation on seismic reflectivity of sand reservoirs encased in shale," *Geophysics*, 39, 759-769.

Dutta, N.C., and Ode, H. (1979). "Attenuation and dispersion of compressional waves in fluid-filled porous rocks with partial gas saturation (White model) - Part I: Biot theory, Part II: Results," *Geophysics*, 44, 1777-1805.

Dutta, N.C., and Ode, H. (1983). "Seismic reflection from a gas-water contact," *Geophysics*, 48, 148-162.

Finn, W.D.L. (1995a). "Evaluation of liquefaction potential by in situ methods," Proc., Earthq. Engr. and Site Char. Workshop, USACE, Waterways Experiment Station, Vicksburg, MS, June 27-28.

Finn, W.D.L. (1995b). "A basis for selecting indicators of liquefaction potential," Proc., Earthq. Engr. and Site Char. Workshop, USACE, Waterways Experiment Station, Vicksburg, MS, June 27-28.

Frenkel, J. (1944). "On the theory of seismic and seismoelectric phenomena in a moist soil," *J. Phys.*, USSR, 8, 230-241.

Gardner, G.H.F., Gardner, L.W., and Gregory, A.R. (1974). "Formation velocity and density: The diagnostic basis for stratigraphic traps," *Geophysics*, 39, 770-780.

Gassmann, F. (1951). "Uber die elastizität poröser medien," *Viert. der. Naturf. Gesell. in Zurich*, 96, 1-23.

Gauthier, O., Tarantola, A., and Virieux, J. (1986). "Two-dimensional nonlinear inversion of seismic waveforms," *Geophysics*, 51, 1387-1403.

Geertsma, J. (1957). "The effect of fluid pressure decline on volumetric changes of porous rocks," *Trans. AIME*, 210, 331.

Geertsma, J., and Smit, D.C. (1961). "Some aspects of elastic wave propagation in fluid-saturated porous solids," *Geophysics*, 26, 169-181.

Geli, L., Bard, P.Y., and Schmitt, D.P. (1987). "Seismic wave propagation in a very permeable water-saturated surface layer," *J. Geophys. Res.*, 92, 7931-7944.

Gelius, L.J. (1995a). "Generalized acoustical diffraction tomography," *Geophys. Prosp.*, 43, 3-30.

Gelius, L.J. (1995b). "Limited-view diffraction tomography in a nonuniform background," *Geophysics*, 60, 580-588.

Gelius, L.J., Johansen, I., Sponheim, N., Stamnes, J.J. (1991). "A generalized diffraction tomography algorithm," *J. Acoust. Soc. Am.*, 89, 523-528.

Gilbert, P. (1972). "Iterative methods for the three-dimensional reconstruction of an object from projections," *J. Theor. Biol.*, 36, 105-117.

Golub, G., and Reinsch, C. (1970). "Singular value decomposition and least-squares solutions," *Numer. Math.*, 14, 403-420.

Han, D., Nur, A., and Morgan, D. (1986). "Effects of porosity and clay content on wave velocities in sandstones," *Geophysics*, 51, 2093-2107.

Harris, M.J. (1987). "Diffraction tomography with arrays of discrete sources and receivers," *IEEE Trans.*, GE-25, 448-455.

Hassanzadeh, S. (1991). "Acoustic modeling in fluid-saturated porous media," *Geophysics*, 56, 424-436.

Helgesen, J., and Kolb, P. (1989). "Inversion of 1-D acoustic medium from real seismic data," Presented at the 59th Ann. Internat. Mtg., *Soc. Expl. Geophys., Expanded Abstracts,* 1000-1003.

Hestenes, M., and Stiefel, E. (1952). "Methods of conjugate gradients for solving linear systems," *Nat. Bur. Standards J. Res.*, 49, 409-436.

Ivansson, S. (1986). "Seismic borehole tomography - Theory and computational methods," *Proc. IEEE*, 74, 328-338.

Kawasumi, H. (1968). "General report on the Niigata earthquake of 1964, Tokyo," Electrical Engineering College Press.

Kelly, K.R., Ward, R.W., Treitel, S., and Alford, R.M. (1976). "Synthetic seismograms: A finite difference approach," *Geophysics*, 41, 2-27.

Kolb, P., Collino, F., and Lailly, P. (1986). "Prestack inversion of a 1D medium," *Proc. IEEE*, 74, 498-506.

Ladas, K.T., and Devaney, A.J. (1991). "Generalized ART-algorithm for diffraction tomography," *Inverse Problems*, 7, 109-125.

Lines, L.R., and LaFehr, T. (1989). "Tomographic modeling of a cross-borehole data set," *Geophysics*, 54, 1249-1257.

Lines, L., and Treitel, S. (1984). "A review of least-squares inversion and its application to geophysical problems," *Geophys. Prosp.*, 32, 159-186.

Lo, T., Duckworth, G.L., and Toksöz, M.N. (1990). "Minimum cross entropy seismic diffraction tomography," *J. Acoust. Soc. Am.*, 87, 748-756.

Lo, T., Toksöz, M.N., Xu, S., and Wu, R.S. (1988). "Ultrasonic laboratory tests of geophysical tomographic reconstruction," *Geophysics*, 53, 947-956.

Mora, P. (1987). "Nonlinear two-dimensional elastic inversion of multi-offset seismic data," *Geophysics*, 52, 1211-1228.

____ (1988). "Elastic wavefield inversion of reflection and transmission data," *Geophysics*, 53, 750-759.

Mavko, G., and Nur, A. (1975). "Melt squirt in asthenosphere," *J. Geophys. Res.*, 80, 1444-1448

____ (1979). "Wave attenuation in partially saturated rocks," *Geophysics*, 44, 161-178.

Mavko, G., and Jizba, D. (1991). "Estimating grain-scale fluid effects on velocity dispersion in rocks," *Geophysics*, 56, 1940-1949.

McAulay, A. (1985). "Prestack inversion with plane-layer point source modeling," *Geophysics*, 50, 77-89.

Moser, T.J. (1991). "Shortest path calculation of seismic rays," *Geophysics*, 56, 59-67.

Murphy, W.F., Winkler, K.W., and Kleinberg, R.L. (1986). "Acoustic relaxation in sedimentary rocks: Dependence on grain contacts and fluid saturation," *Geophysics*, 51, 757-766.

Nazarian, S., and Stokoe, K.H. II (1984). "In situ shear wave velocities from spectral analysis of surface waves," Proc. 8th World Conf. on Earthq. Engr. , San Francisco, CA, III, 31-28.

Nolet, G. (1987a). "Seismic Tomography," Guust Nolet Ed., D. Reidel Pub. Co.

Nolet, G. (1987b). "Waveform tomography," in Seismic Tomography, Guust Nolet Ed., D. Reidel Pub. Co., 301-322.

Ogushwitz, P.R. (1985). "Applicability of the Biot theory. I. Low-porosity materials," *J. Acoust. Soc. Am.*, 77, 429-440.

Paige, C.C., and Saunders, M.A. (1982). "LSQR: An algorithm for sparse linear equations and sparse least squares," *ACM Trans. Math. Softw.*, 8, 43-71.

Pan, G.S., and Phinney, R.A., and Odom, R.I. (1988). "Full-waveform inversion of plane-wave seismograms in stratified acoustic media: Theory and feasibility," *Geophysics*, 53, 21-31.

Pan, G.S., and Phinney, R.A. (1989). "Full-waveform inversion of plane-wave seismograms in stratified acoustic media: Applicability and limitations," *Geophysics*, 54, 568-580.

Pica, A., Tarantola, A., and Diet, J.P. (1990). "Nonlinear inversion of seismic reflection data in a laterally invariant medium," *Geophysics*, 55, 284-292.

Plona, T.J. (1980). "Observation of a second bulk compressional wave in a porous medium at ultrasonic frequencies," *Appl. Phys. Lett.*, 36, 259-261.

Podvin, P., and Lecomte, I. (1991). "Finite difference computation of traveltimes in very contrasted velocity models: A massively parallel approach and its associated tools," *Geophys. J. Int.*, 105, 271-284.

Pratt, R.G., and Worthington, M.H. (1988). "The application of diffraction tomography to crosshole seismic data," *Geophysics*, 53, 1284-1294.

Rasolofosaon, P.N.L. (1987). "New experimental evidence of the influence of permeability on acoustic wave propagation: Attenuation of ultrasonic guided waves in rock plates," 57th Ann. Inter. Mtg. , *Soc. Expl. Geophys. Extended Abstracts*, 670-673.

Rechtien, R.D., and Ballard, R.F., Jr. (1993). "Cross-borehole seismic tomographs of tunnels, "Proc. Fourth Tunnel Detection Symp. on Subsurface Expl. Tech., Golden CO, pp333-343.

Rechtien, R.D., Hambacker, K.L., and Ballard, R.F., Jr. (1993). "A high-frequency sparker source for the borehole environment," *Geophysics*, 58, 660-669.

Robertson, P.K. (1990). "Seismic cone penetration testing for evaluation of liquefaction potential," Proceedings, Symp. on Recent Advances in Earthquake Design Using Laboratory and In situ Tests, ConeTec Investigations Ltd., Burnaby, BC, February 5.

Rosenbaum, J.H. (1974). "Synthetic microseismograms: Logging in porous formations," *Geophysics*, 39, 14-32.

Scales, J.A., Gersztenkorn, A., and Treitel, S. (1988). "Fast l_p solution of large, sparse, linear sytems: Application to seismic traveltime tomography," J. *Comput. Phys.*, 75, 314-333.

Schmitt, D.P., Bouchon, M., and Bonnet, G. (1988). "Full-wave synthetic logs in radially semi-infinite saturated porous media," *Geophysics*, 53, 807-823.

Schneider, W.A., Jr., Ranzinger, K. A., Balch, A. H., and Kruse, C. (1992). "A dynamic programming approach to first-arrival traveltime computation in media with arbitrarily distributed velocities," *Geophysics*, 57, 39-50.

Schneider, W.A., Jr. (1995). "Robust and efficient upwind finite-difference traveltime calculations in three dimensions," *Geophysics*, 60, 1108-1117.

Seed, H.B. et al. (1990). "Preliminary report on the principal geotechnical aspects of the October 17, 1989 Loma Prieta earthquake," Report No. UCB/EERC-90)-05, University of California, Berkeley.

Sen, M.K., and Stoffa, P.L. (1991). "Nonlinear one-dimensional seismic waveform inversion using simulated annealing," *Geophysics*, 56, 1624-1638.

Sirles, P.C. (1987). "Shear-wave velocity and attenuation anaysis of liquefiable soils in the south Truckee Meadows, Washoe County, Nevada," M.S. Thesis, University of Nevada, Reno.

Stokoe, K.H., and Hoar, R.J. (1978). "Variables affecting in situ seismic measurements," Proc. ASCE Geotech. Eng. Div., Specialty Conf. on Earthq. Eng. & Soil Dynamics, Park City, Utah, ASCE 2 919-939.

Stoll, R.D. (1974). "Acoustic waves in saturated sediments,"*Physics of sound in marine sediments*, L. Hampton Ed., Plenum Press.

____ (1977). "Acoustic waves in ocean sediments," *Geophysics*, 42, 715-725.

____ (1980). "Theoretical aspects of sound transmission in sediments," *J. Acoust. Soc. Am.*, 68, 1341-1350.

____ (1985). "Marine sediments acoustics," *J. Acoust. Soc. Am.*, 77, 1789-1799.

Stoll, R.D., and Bryan, G.M. (1970). "Wave attenuation in saturated sediments," *J. Acoust Soc. Am.*, 47, 1440-1447.

Stoll, R.D., and Kan, T.-K. (1981). "Reflection of acoustic waves at a water-sediment interface," *J. Acoust. Soc. Am.*, 70, 149-156.

Symes, W.W., and Carazzone, J. J. (1991). "Velocity inversion by differential semblance optimization," *Geophysics*, 56, 654-663.

Tien, L.-W, and Inderwiesen, P. (1994). "Fundamentals of seismic tomography," Geophysical Monograph No. 6, Soc. Expl. Geophysics.

Tanabe (1971). "Projection method for solving a singular system of linear equations and its applications," *Numer. Math.*, 17, 203-214.

Tarantola, A. (1984). "The seismic reflection inverse problem," *Inverse Problems of Acoustic and Elastic Waves,* F. Santosa, Y.-H. Pao, W.W. Symes, and C. Holland, Eds., Soc. Ind. Appl. Math.

____ (1986). "A strategy for nonlinear elastic inversion of seismic reflection data," *Geophysics*, 51, 1893-1903.

____ (1987a). "Travel time and seismic waveform inversion," *Seismic Tomography,* Guust Nolet Ed., D. Reidel Pub. Co., 135-158.

____ (1987b). "Inverse problem theory: Methods for data fitting and parameter estimation," Elsevier Science Publ.

Tarantola, A., and Vallette, B. (1982). "Generalized nonlinear inverse problems solved using the least squared criterion," *Rev. Geophys. Space Phys.*, 20, 219-232.

Tura, M.A.C., Johnson, L.R., Majer, E.L., and Peterson, J.E. (1992). "Application of diffraction tomography to fracture detection," *Geophysics*, 57, 245-257.

Turgut, A. , and Yamamoto, T. (1988). "Synthetic seismograms for marine sediments and determinations of porosity and permeability," *Geophysics*, 53, 1056-1067.

van Trier, J., and Symes, W.W. (1991). "Upwind finite difference calculation of traveltimes," *Geophysics*, 56, 812-821.

Vidale, J.E. (1990). "Finite difference calculation of traveltimes in three dimensions," *Geophysics*, 55, 521-526.

Wang, Z., and Nur, A. (1990). "Dispersion analysis of acoustic velocities in rocks," *J. Acoustic. Soc. Am.*, 87, 2384-2395.

Winkler, K.W., Plona, T.J., Froelich, B., and Liu, H.-L. (1987). "Borehole Stoneley waves and permeability: Laboratory results," 57th Ann. Inter. Mtg., Soc. Expl. Geophys., Expanded Abstracts, 12-13.

Woods, R.D. (1991). "Field and laboratory determination of soil properties at low and high strains," Proc. 2nd Internat. Conf. on Recent Advances in Geotech. Earthq. Engr. and Soil Dynamics, St. Louis, Mo. 1727-1741.

Wu, R.S., and Toksöz, M.N. (1987). "Diffraction tomography and multisource holography applied to seismic imaging," *Geophysics*, 52, 11-25.

Yamamoto, T. (1983). "Acoustic propagation in the ocean with a poroelastic bottom," *J. Acoust. Soc. Am.*, 73, 1587-1596.

Yamamoto, T., and Turgut, A. (1988). "Acoustic wave propagation through porous media with arbitrary pore size distributions," *J. Acoust. Soc, Am.*, 83, 1744-1751.

Yamamoto, T., Trevorrow, M., Badiey, M., and Turgut, A. (1989). "Seabed porosity and shear modulus inversion using surface gravity (water) wave-induced seabed motion," *Geophys. J. Int.*, 98, 173-182.

Yamamoto, T., Nye, T., and Kuru, M. (1994). "Porosity, permeability, shear strength: Crosswell tomography below an iron foundry, " *Geophysics* 59, 1530-1541.

Yamamoto, T., Nye, T., and Kuru, M. (1995), "Imaging the permeability structure of a limestone aquifer by crosswell acoustic tomography," *Geophysics*, 60, 1634-1645.

Zhu , X., and McMechan, G.A. (1991). "Finite difference modeling of the seismic response of fluid-saturated, porous, elastic media using Biot theory," *Geophysics*, 56, 328-339.

Zienkiewicz, O.C., and Shiomo, T. (1984). "Dynamic behavior of saturated porous media: the generalized Biot formulation and its numerical solution," *Int. J. Num. Anal. Meth. in Geomech.*, 8, 71-96.

REPORT DOCUMENTATION PAGE

Form Approved
OMB No. 0704-0188

1.AGENCY USE ONLY *(Leave blank)*

2.REPORT DATE
August 1996

3.REPORT TYPE AND DATES COVERED
Final report

4.TITLE AND SUBTITLE
In Situ Seismic Investigation of Liquefaction Potential of Soils

5.FUNDING NUMBERS
Contract DACW39-95-M-2999
Work Unit 33014

6.AUTHOR(S)
Richard D. Rechtien

7.PERFORMING ORGANIZATION NAME(S) AND ADDRESS(ES)
Consulting Geophysicist
15040 County Road 8160
Rolla, MO 65401

8.PERFORMING ORGANIZATION REPORT NUMBER

9.SPONSORING/MONITORING AGENCY NAME(S) AND ADDRESS(ES)
U.S. Army Corps of Engineers,
Washington, DC 20314-1000;
U.S. Army Engineer Waterways Experiment Station,
3909 Halls Ferry Road, Vicksburg, MS 39180-6199

10.SPONSORING/MONITORING AGENCY REPORT NUMBER
Contract Report
GL-96-1

11.SUPPLEMENTARY NOTES
Available from the National Technical Information Service, 5285 Port Royal Road, Springfield, VA 22161.

12a.DISTRIBUTION/AVAILABILITY STATEMENT
Approved for public release; distribution is unlimited.

12b.DISTRIBUTION CODE

13.ABSTRACT *(Maximum 200 words)*

This report examines the use of exploratory seismic technology as a tool for measurement of in situ liquefaction potential of saturated, cohesionless soils. Past appplications of seismic technology have focused principally on shear velocity as a liquefaction indicator. Inherent in these applications was the assumption of a nonporous, perfectly elastic media; the theory of which provides simple procedures for conversion of combined measurements of distance and travel time to "shear velocity." This property, dependent on shear modulus and density of a perfectly elastic solid, is all that can be produced experimentally because of the simplicity of the assumed earth model used as basis for interpretation.

All interpretive geophysical approaches require use of conceptual earth models. For the liquefaction problem, the key to success is choice of a model that incorporates dynamic attributes of fluid-saturated, noncohesive sediments. A Biot model, modified to include fracture porosity and permeability, is proposed as a proper choice. Consequently, assignment of combinations of measured particle motion attributes to earth model parameters must be reevaluated in light of the Biot theory.

A field experiment is proposed with the Biot model and waveform tomography in mind. This experiment embodies concepts relative to current and future data processing capabilities.

14.SUBJECT TERMS
Biot
Liquefaction
Seismic
Soils
Tomography

15.NUMBER OF PAGES
46

16.PRICE CODE

17.SECURITY CLASSIFICATION OF REPORT	18.SECURITY CLASSIFICATION OF THIS PAGE	19.SECURITY CLASSIFICATION OF ABSTRACT	20.LIMITATION OF ABSTRACT
UNCLASSIFIED	UNCLASSIFIED		